Vulnerability of Dopaminergic Amacrine Cells to Chronic Ischemia in a Mouse Model of Oxygen-Induced Retinopathy

Nathan J. Spix,[1] Lei-Lei Liu,[1] Zhijing Zhang,[2] Joshua P. Hohlbein,[1] Cameron L. Prigge,[1] Shravan Chintala,[1] Christophe P. Ribelayga,[2,3] and Dao-Qi Zhang[1]

[1]Eye Research Institute, Oakland University, Rochester, Michigan, United States
[2]Ruiz Department of Ophthalmology and Visual Science, McGovern Medical School, The University of Texas Health Science Center at Houston, Houston, Texas, United States
[3]Graduate School of Biomedical Sciences, The University of Texas Health Science Center at Houston, Houston, Texas, United States

Correspondence: Dao-Qi Zhang, Eye Research Institute, Oakland University, 423 Dodge Hall, Rochester, MI 48309, USA; zhang@oakland.edu.

Submitted: February 15, 2016
Accepted: May 9, 2016

Citation: Spix NJ, Liu L-L, Zhang Z, et al. Vulnerability of dopaminergic amacrine cells to chronic ischemia in a mouse model of oxygen-induced retinopathy. *Invest Ophthalmol Vis Sci*. 2016;57:3047–3057. DOI:10.1167/iovs.16-19346

Purpose. Retinal dopamine deficiency is a potential cause of myopia and visual deficits in retinopathy of prematurity (ROP). We investigated the cellular mechanisms responsible for lowered levels of retinal dopamine in an oxygen-induced retinopathy (OIR) mouse model of ROP.

Methods. Retinopathy was induced by exposing mice to 75% oxygen from postnatal day 7 (P7) to P12. Oxygen-induced retinopathy and age-matched control mice were euthanized at P12, P17, P25, or P42 to P50. Immunohistochemistry, electrophysiology, and biochemical approaches were used to determine the effect of OIR on the structure and function of dopaminergic amacrine cells (DACs).

Results. The total number of DACs was unchanged in OIR retinas at P12 despite significant capillary dropout in the central retina. However, a significant loss of DACs was observed in P17 OIR retinas (in which neovascularization was maximal), with the cell loss being more profound in the central (avascular) than in the peripheral (neovascular) regions. Cell loss was persistent in both regions at P25, at which time retinal neovascularization had regressed. At P42, the percentage of DACs lost (54%) was comparable to the percent decrease in total dopamine content (53%). Additionally, it was found that DACs recorded in OIR retinas at P42 to P50 had a complete dendritic field and exhibited relatively normal spontaneous and light-induced electrical activity.

Conclusions. The results suggest that remaining DACs are structurally and functionally intact and that loss of DACs is primarily responsible for the decreased levels of retinal dopamine observed after OIR.

Keywords: dopamine, amacrine cells, retinal degeneration, retinopathy of prematurity

Dopamine is a key neuromodulator in the retina and has an important role in eye development and visual function.[1,2] Dopamine deficiency has been observed in a number of eye diseases, including retinopathy of prematurity (ROP), a potentially blinding disease that affects premature infants. This deficiency is likely to be associated with the refractive errors of the eye, and visual deficits detected in patients with mild ROP as well as in ROP animal models.[3–5] However, the cellular mechanisms by which ROP causes decreased levels of retinal dopamine are unclear.

The sole source of dopamine in the retina is a specialized subclass of amacrine cells, the dopaminergic amacrine cells (DACs). Approximately 500 DACs are distributed sparsely and regularly across the mouse retina.[6] Their dendrites and axon-like processes overlap extensively, forming a dense network in the inner plexiform layer (IPL). Some axon-like processes also traverse the inner nuclear layer (INL) toward the outer retina, forming clusters of fine processes in the outer plexiform layer (OPL). Thus, DACs can be classified as interplexiform cells, providing an intraretinal feedback pathway that transmits visual signals against the canonical pathways, from the inner retina back to the outer retina.[1] This specialized feature of DACs has been considered a potential structural basis for the oscillatory potentials observed in the electroretinogram (ERG), a noninvasive electrophysiologic method for studying retinal function.[7–9]

Reduction in amplitude of ERG oscillatory potentials (Ops) in OIR implicates possible structural and functional abnormality of DACs.[9] Structural alterations of DACs in the rat model of oxygen-induced retinopathy (OIR) have been examined using an antibody against tyrosine hydroxylase (TH), the rate-limiting enzyme in dopamine biosynthesis, but the reported results are inconsistent.[3,10] Downie et al.[10] have demonstrated that the number of DACs remains unchanged in retinas with OIR, whereas Zhang et al.[3] reported that a loss of DAC processes occurs in a similar rat model.[3] However, the latter study did not attempt to count the number of DACs during the development of OIR. Thus, it is unclear whether the reported loss of processes is due to downregulation of TH immunoreactivity, cell death, or decreased dendritic and axonal ramification of DACs.

It also is unknown whether OIR affects the electrical activity (action potentials) of DACs, which would, in turn, lead to a reduction in retinal dopamine (since the action potentials of DACs are associated with dopamine release). We previously have demonstrated that DACs in wild-type retinas exhibit spontaneous action potentials in darkness and an elevated number of action potentials during illumination.[11] A similar approach can be adopted to determine whether the spontaneous and light-evoked activity of DACs are altered in OIR retinas.

The present study focuses on addressing the above unresolved issues using a mouse model of OIR, a popular model of human ROP.[12] The mouse model of OIR exhibits two distinct phases, similar to ROP: vaso-obliteration (phase I) and neovascularization (phase II).[12] This model has the advantage of allowing the use of a transgenic mouse in which DACs are genetically labeled with red fluorescent protein (RFP), facilitating morphologic and physiologic studies of these cells.[13] We reported that the number of DACs remains unchanged in phase I but substantially decreases in phase II, with this reduction persisting after regression of neovascularization. We also described the effect of OIR on TH immunoreactivity, the total content of dopamine and its metabolite 3,4-dihydroxyphenylacetic acid (DOPAC), and the morphologic and physiologic profiles of individual surviving DACs.

Materials and Methods

Animals

Wild-type C57BL/6 mice were obtained from the Jackson Laboratory (Bar Harbor, ME, USA). Transgenic mice in which DACs are labeled with RFP under the control of the TH promoter were originally bred at Vanderbilt University.[13] The mice were housed in a 12/12-hour light/dark cycle at Oakland University's Biomedical Research Support Facility. Food and water were given ad libitum. All procedures were performed in accordance with the National Institutes of Health (NIH) guidelines for work with laboratory animals and the ARVO Animal Statement for the Use of Animals in Ophthalmic and Vision Research, and were approved by the Institutional Animal Care and Use Committee at Oakland University.

Oxygen-Induced Retinopathy

To induce retinopathy, cages containing 7-day-old litters and their dams were transferred to a sealed Plexiglas chamber. The oxygen level inside the chamber was maintained at 75% using a ProOx P110 oxygen controller (BioSpherix, New York, NY, USA). Sodasorb (W. R. Grace & Co., Columbia, MD, USA) was placed into the chamber to absorb excess carbon dioxide. After 5 days of treatment, the litter was returned to normal housing conditions (room air). Since oxygen treatment often caused severe stress to the nursing dam, a surrogate dam was substituted to allow the biological dam to recover. Control mice were maintained in room air during the entire postnatal period. Totally, 61 OIR and 52 age-matched control mice were used for the present study.

Immunohistochemistry

For all experiments performed in the present study, mice were euthanized by asphyxiation with CO_2 followed by cervical dislocation. Immediately after euthanasia, both eyes were enucleated and fixed in 4% paraformaldehyde (Sigma-Aldrich Corp., St. Louis, MO, USA). After fixation, the retinas were dissected from the eyecups for whole mount immunostaining.

Whole retinas were blocked for 2 hours with 1% BSA (Fisher Scientific, Hampton, NH, USA) and 0.3% Triton-X 100 (Sigma-Aldrich Corp.) in 0.1 × PBS. Retinas were incubated with primary antibodies against TH (1:1000; AB1542; EMD Millipore, Billerica, MA, USA) or choline acetyltransferase (1:500; AB 144P; EMD Millipore). For some experiments, isolectin GS-IB_4 (1:100; I21411; Life Technologies, Carlsbad, CA, USA) was added before day 2 of incubation to stain the retinal vasculature. Retinas then were rinsed in 0.1 × PBS and incubated for 2 hours with secondary antibodies raised in donkey, conjugated to AlexaFluor-488 or 594 (1:500; Life Technologies). Finally, whole retinas were mounted on slides with Vectashield Hard-Set mounting solution (Vector Laboratories, Burlingame, CA, USA).

Imaging and Analysis

Whole mount retinas were visualized on a Zeiss Axio Imager.Z2 fluorescence microscope, using Zeiss AxioVision software to collect images (Zeiss, Oberkochen, Germany). The MosaiX function was used to obtain tile scan images of the entire retina at ×10 or ×20 magnification. Then, NIS Elements AR software (Nikon Instruments, Inc., Tokyo, Japan) was used to stitch tile images into a single large image. In a few cases where this software was unable to produce a satisfactory result, the stitching plugin for Fiji developed by Stephen Preibisch was used.[14]

Dopaminergic amacrine cells expressing TH were counted manually using the Cell Counter plugin for Fiji (version 2, developed by Kurt DeVos), which recorded the location of each cell in a Cartesian coordinate system. The location of the optic nerve head also was recorded, and the distance from each cell to the optic nerve head. For each retina, the distance between the optic nerve head and the cell farthest from the optic nerve head was considered to be the maximum radius. Each retina then was divided into central and peripheral regions based on its maximum radius: a circle centered on the optic nerve head with half the maximum radius delineated the boundary between the central and peripheral retina.

The area of each retina was measured with Fiji, using the following procedure: Whole mount images of the retina were segmented using Automatic Threshold. Nonretinal image artifacts then were subtracted manually from the selection. The retina was divided into central and peripheral regions as described above, and the area of each region was calculated. Regional cell density was calculated by dividing the number of cells in each region by the area of that region.

Fluorescence images of whole mount retinas were processed further in Fiji to allow for clear presentation of results. Automatic Thresholding (triangle and default methods) was used to delineate the outer boundary of the retina in images of retinas stained with anti-TH. The recorded locations of DACs then were superimposed on the outline of the retina using Adobe Photoshop (Adobe Systems, San Jose, CA, USA). In addition, for retinas stained with isolectin GS-IB_4, sliding paraboloid background removal was applied before thresholding to segment the retinal vasculature. This image then was overlaid onto the outline of the retina, and DAC locations were superimposed as described above. Final colorization of images was performed using Adobe Photoshop Elements.

Western Blot Analysis

For each sample, four retinas were pooled together in an Eppendorf tube containing 60 μL of extraction buffer (1% Nonidet-P40, 20 mM Tris-HCl, 150 mM NaCl, 1 mM Na_3VO_4, pH 7.4) with protease inhibitors, and the tissues were homogenized. Retinal tissue homogenates were centrifuged

Investigative Ophthalmology & Visual Science

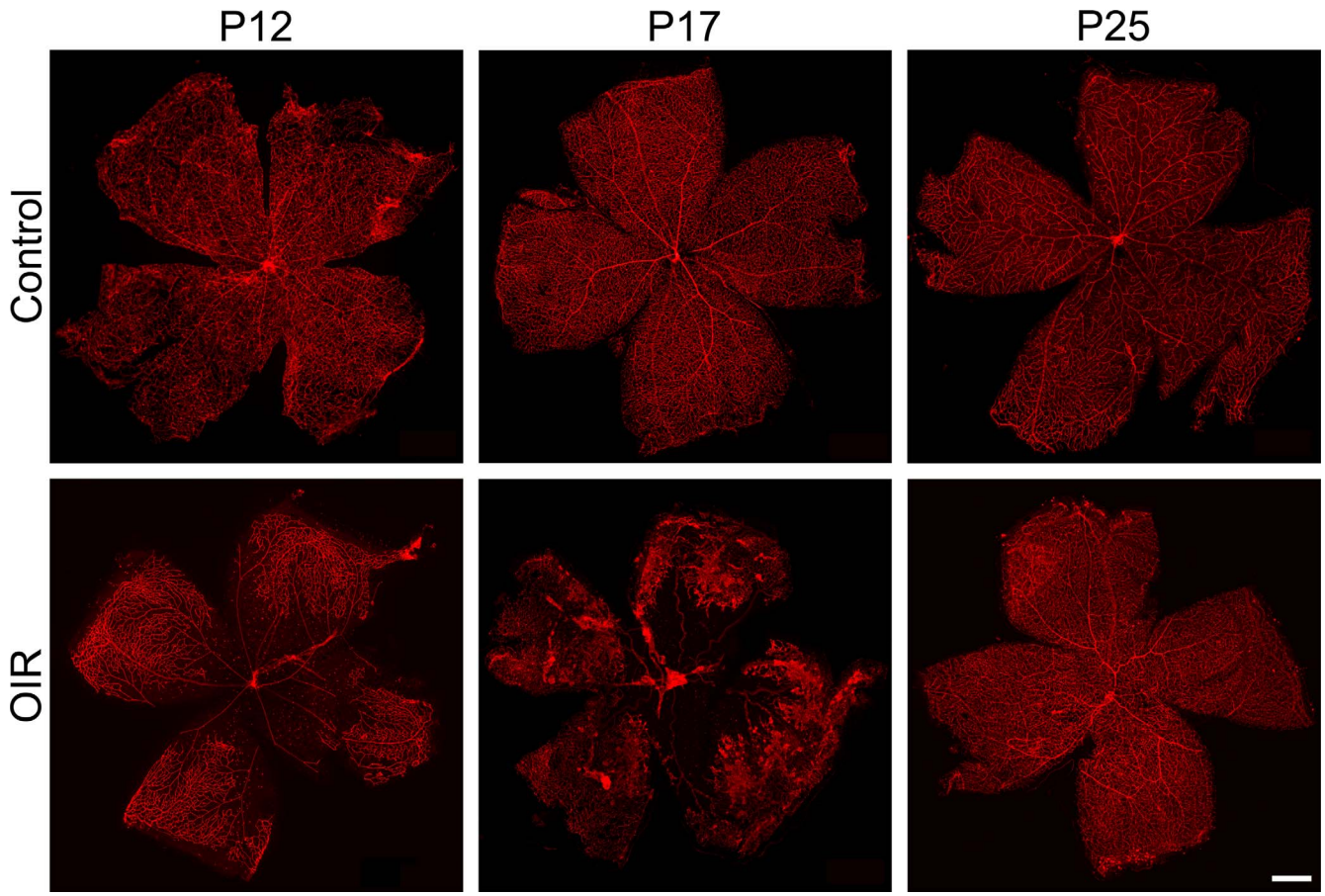

Figure 1. Retinal vasculature during normal development and OIR. *Left*, significant capillary dropout in the central OIR at P12 (*bottom*), while the control retina (*top*) exhibits normal vascularization throughout. *Middle*, extensive neovascularization in the OIR retina (*bottom*) but not in the control retina (*top*) at P17. *Right*, illustrates that by P25, neovascularization had regressed in the OIR retina (*bottom*), which appeared quite similar to the control retina (*top*). *Scale bar*: 500 μm.

at 7840*g* for 5 minutes at 4°C, and the supernatants were collected. The protein concentration of each of the samples was determined using a Bio-Rad protein assay kit (Bio-Rad Laboratories, Hercules, CA, USA).

Aliquots containing 50 μg of protein were mixed with gel loading buffer and separated using 10% SDS-PAGE. After electrophoresis, the proteins were transferred onto Immobilon-FL membranes (EMD Millipore) and nonspecific binding sites were blocked with Odyssey blocking buffer containing 0.2% Tween 20 (TBS-T). After incubating with primary antibodies against TH (1:2500; MAB318, EMD Millipore) and actin (1:2500 dilution), membranes were washed with TBS-T and incubated with appropriate secondary antibodies conjugated to IRDye 700 or 800 (LI-COR, Lincoln, NE, USA) for 1 hour at room temperature. Finally, the membranes were scanned using an Odyssey two-channel IR-detection scanner (LI-COR). Image analysis was done using Image Studio (LI-COR).

Patch-Clamp Recordings

Eyes were enucleated under infrared illumination, then transferred to a petri dish filled with oxygenated extracellular solution containing (in mM) 125 NaCl, 2.5 KCl, 1 $MgSO_4$, 2 $CaCl_2$, 1.25 $NaHPO_4$, 20 glucose, and 26 $NaHCO_3$. The cornea and lens were removed from the eye and the retina was separated from the sclera under a dim red light. The retina then was placed photoreceptor side down in a recording chamber mounted on the stage of an upright conventional fluorescence microscope (Axio Examiner; Zeiss). Oxygenated extracellular medium (pH 7.4 with 95% O_2–5% CO_2) continuously perfused the recording chamber at a rate of 2 to 3 mL/min, and the superfusate was maintained at 32°C to 34°C by a temperature control unit (TC-344B; Warner Instruments, Hamden, CT, USA).

TH::RFP-expressing cells were first identified using a fluorescence microscope with a rhodamine filter set and an excitation wavelength of 535 nm. The identified cells and glass electrodes then were visualized using infrared differential interference contrast (IR-DIC) optics. Cell-attached recordings were made from the soma of RFP-labelled DACs with 4 to 8 MΩ electrodes, and signals were amplified with an Axopatch 200B amplifier (Molecular Devices, Sunnyvale, CA, USA). The pipette solution contained 150 mM NaCl and 10 mM HEPES adjusted to pH 7.4 with NaOH. Data were acquired via a Digidata 1440A digitizer (Molecular Devices) and analyzed offline using Clampex 10 software (Molecular Devices).

Light stimuli were generated using a light-emitting diode (LED) with a peak wavelength of 470 nm (LED Supply, Randolph, VT, USA; and L.C. Corp, Brooklyn, NY, USA). An LED controller (Mightex, Pleasanton, CA, USA) was used to drive the LED and the light intensity was adjusted by varying the driving current. The photon flux (photons/s/cm^2) were measured at the surface of the retina. Data were analyzed using the Clampfit 10 software.

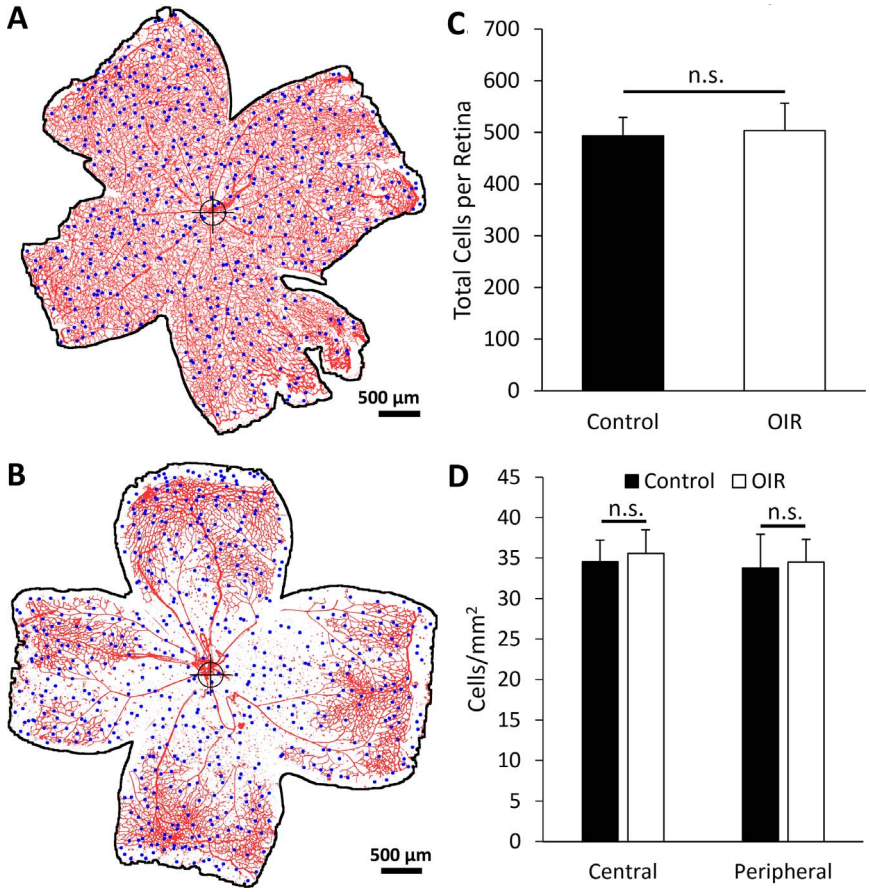

Figure 2. Total number and distribution of DACs in OIR remains unchanged at P12. (**A**, **B**) Tracings of whole mount retinas taken from the control and OIR groups, respectively. *Blue dots* represent DACs, while *red lines* represent blood vessels. The *black border* represents the boundary of the retina as mounted on the slide, and the *crossbairs* denotes the center of the optic nerve. Despite significant capillary dropout in the central region of the OIR retina (**B**), the total number of DACs in OIR was unchanged compared to the control retina (**A**). Averaged data are shown in (**C**). Furthermore, the densities of DACs in the central and peripheral regions of the OIR retina were similar to those observed in the control retina (**D**).

Dye Injection

Dye injection into DACs was performed using the same setup as for patch-clamp recording (described above). Sharp electrodes were filled with Lucifer yellow (Sigma-Aldrich Corp.) and neurobiotin (Vector Laboratories). After penetration, the cells were filled by inducing amplifier oscillation via overcompensation for 2 to 3 minutes. Whole retinas then were stained with streptavidin/fluorophore conjugate (1:200; Vector Laboratories) to allow for visualization of neurobiotin. Injected cells were visualized as above and traced using the Simple Neurite Tracer plugin for Fiji.[15] The total dendritic length was measured, as well as the area of the dendritic field.

Dopamine and DOPAC Measurement

Reversed-phase HPLC with electrochemical detection (ED) was used to assay dopamine and its metabolite DOPAC. The liquid chromatograph and detection system consisted of a Prominence HPLC (Shimadzu Scientific Instruments, Columbia, MD) with a Hypersil ODS C18 column (250 × 4.6 mm, 5-µm porous silica, ThermoScientific, Grand Island, NY, USA) and an amperometric detector (Model LC-4C; BioAnalytical System, West Lafayette, IN, USA). An isocratic mobile phase was used which was composed of 50 mM KH_2PO_4, 0.015% octyl sodium sulphate (ACROS Organics, NJ, USA), and 0.1 mM Na_2-EDTA, which was adjusted to pH 3.10 before adding 13% methanol. The solution then was filtered on a membrane filter (pore size 0.2 µm) and degassed with helium. The mobile phase flow rate was set to 1 mL/min, and the column temperature was set to 30°C. The potential of the working carbon electrode was set to +0.600 V. The analyzed substances were identified by their relative retention times compared to those of standards and were quantified based on the peak area. The detection threshold of the HPLC system was 5 pg per run, which was determined with a standard solution.

To determine DOPAC and dopamine content, eyes were enucleated, rapidly frozen in liquid nitrogen, and kept at –80°C until assayed. Frozen eyes were homogenized by sonication in 200 µL of a solution containing 0.4 M perchloric acid, 0.1 mM $Na_2S_2O_5$, and 0.1 mM Na_2-EDTA. The homogenate then was centrifuged (30 minutes, 16,000*g*, 4°C), and the supernatant was passed through a 0.2 µm filter. For each sample, 5 µL of supernatant was injected directly into the HPLC system.

Statistical Analyses

Data representing two independent groups were compared using Student's *t*-test. One-way ANOVA was used to determine whether there were any significant differences between the means of more than two independent groups. $P < 0.05$ was

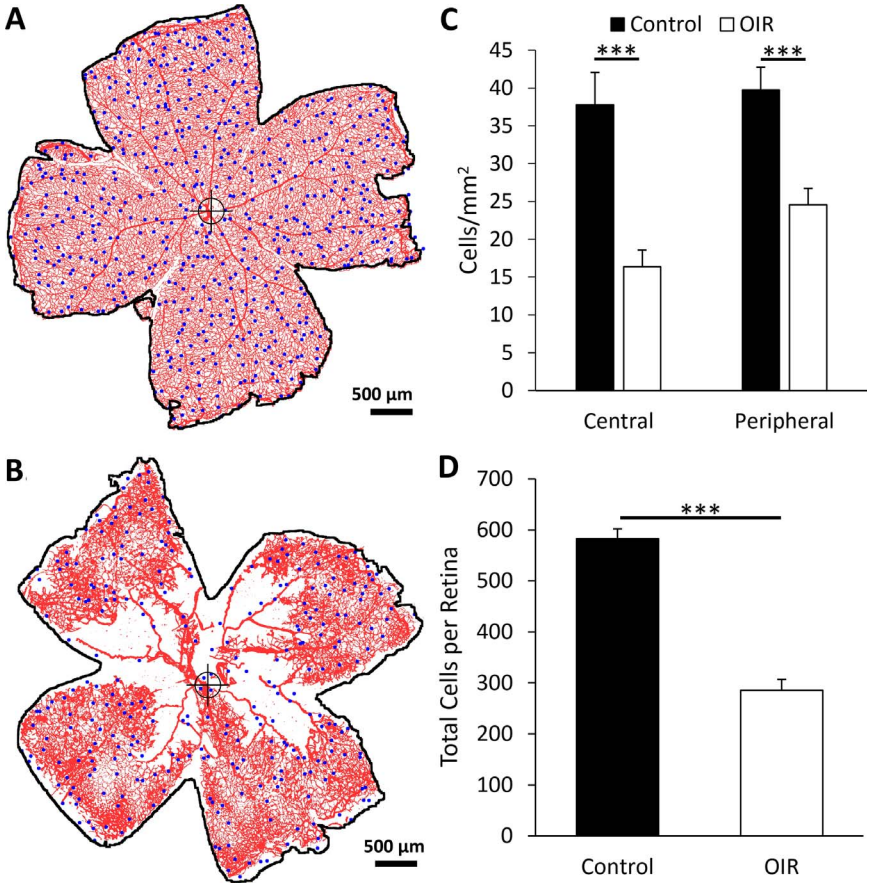

Figure 3. Loss of DACs in OIR at P17. (**A**, **B**) Tracings of whole mount retinas taken from the control and OIR groups, respectively. *Blue dots* represent DACs, while *red lines* represent blood vessels. The *black border* represents the boundary of the retina as mounted on the slide, and the *crosshairs* denotes the center of the optic nerve. Dopaminergic amacrine cells were regularly distributed throughout the control retina at P17 (**A**), but a significant loss of DACs was observed in the OIR retina, especially in the avascular areas (**B**). The OIR group exhibited significant reductions in DAC cell density in the central and peripheral retinal areas, with a greater decrease observed in the central retina (**C**). The total number of DACs in OIR retinas was decreased by 51% compared to control retinas (**D**).

considered statistically significant. Data are presented as the mean ± SD.

Results

To confirm that the OIR model had been successfully implemented, retinas from oxygen-treated and age-matched control mice were immunostained with isolectin GS-IB_4. Representative results from these experiments are shown in Figure 1. At P12, significant capillary dropout was observed in the central area of retinas with OIR, while the peripheral retina appeared normal. Significant neovascularization of the peripheral retina was observed in P17, with the central retina remaining mostly avascular. Neovascularization was observed to regress spontaneously between P17 and P25. These observations confirmed the successful implementation of the OIR model.[12]

To determine whether OIR-induced ischemia (caused by capillary dropout in the central retina at and before P12) resulted in the degeneration of DACs, we performed immunostaining of whole-mount retinas isolated from pups immediately after they were removed from a 75% oxygen environment. We used an anti-TH antibody that can immunolabel two types of catecholaminergic cells in retinas from young animals.[16] One type, the DACs, have a relatively large soma and two to three primary dendrites exhibiting bright TH immunoreactivity. Type II catecholaminergic cells have a relatively small soma size and one primary dendrite with weak but detectable TH staining. For the present study, we counted and analyzed only TH-expressing DACs.

At P12, we found that TH-expressing DACs were distributed evenly throughout the control (Fig. 2A) and OIR retinas (Fig. 2B). The total number of cells was similar in retinas with (503 ± 53 cells, $n = 9$) and without (493 ± 35 cells, $n = 9$; $P = 0.650$; Fig. 2C) OIR. To further investigate the distribution of DACs, we divided each retina into central and peripheral regions. The cell density was measured in both regions and no significant differences in cell density were observed between control ($n = 7$) and OIR ($n = 8$) retinas, either in the central (control, 34.5 ± 2.7 cells/mm^2 versus OIR, 35.6 ± 2.9 cells/mm^2; $P = 0.471$; Fig. 2D) or peripheral retinal areas (control, 33.8 ± 4.2 cells/mm^2 versus OIR, 34.5 ± 2.8 cells/mm^2; $P = 0.700$; Fig. 2D).

At P17, however, few DACs were visible in the central (avascular) retinas of oxygen-treated mice (Fig. 3B). The cell density in the center region (16.4 ± 2.2 cells/mm^2, $n = 9$) was reduced by 57% compared to control retinas (37.8 ± 4.3 cells/mm^2, $n = 12$; $P < 0.001$; Fig. 3C). In the peripheral OIR retina, which was mostly vascular (Fig. 3B), the density of TH-positive DACs (24.5 ± 2.2 cells/mm^2, $n = 9$) was significantly higher

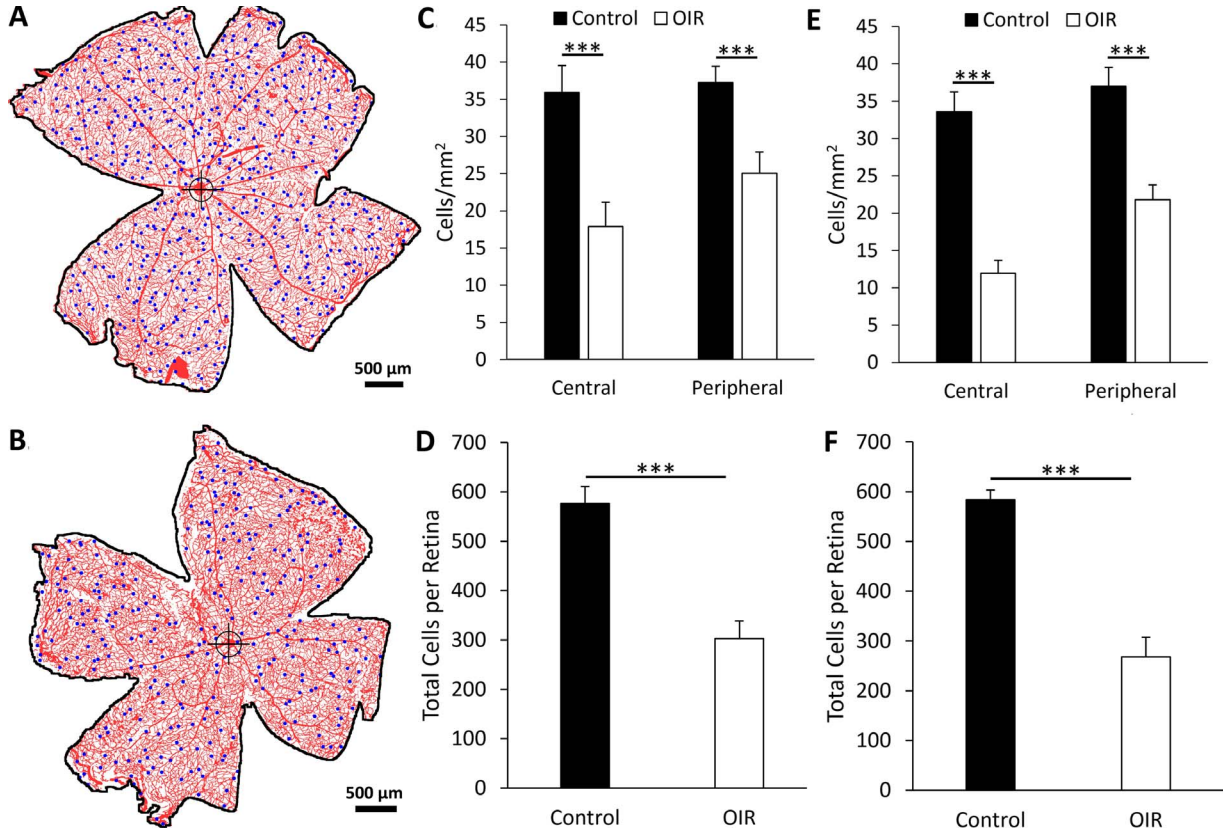

FIGURE 4. Loss of DACs in OIR persists at P25 and P42. (**A**, **B**) are tracings of whole mount retinas taken from the control and OIR groups, respectively. *Blue dots* represent DACs, while *red lines* represent blood vessels. The *black border* represents the boundary of the retina as mounted on the slide, and the *crossbairs* denotes the center of the optic nerve. Compared to the control retina (**A**), significant DAC loss was visible in OIR retinas at P25 despite the fact that the retinal vasculature had returned to normal (**B**). As in P17, while DAC density was reduced in OIR in the central and peripheral retinal areas, a larger decrease was observed in the central retina (**C**). The total number of DACs in OIR retinas was again decreased by 47% compared to control retinas (**D**). Similar results were noted in P42, with consistently low cell densities noted for the OIR group in the central and peripheral retinal areas (**E**). At P42, the total number of DACs in OIR retinas was decreased by 54% compared to control retinas (**F**).

than in the central retina ($P < 0.001$), but still significantly lower than the corresponding area in the control retinas (39.8 ± 3.0 cells/mm^2, $n = 12$; $P < 0.001$; Fig. 3C). Altogether, a 51% decrease in the total number of cells was observed in OIR retinas (285 ± 21 cells; $n = 9$), compared to the control group (583 ± 19 cells, $n = 12$; $P < 0.001$; Fig. 3D).

To determine if the loss of TH-expressing DACs was reversed after the retinal vasculature returned to normal, we examined the number and distribution of DACs at P25 (Figs. 4A, 4B). We observed a 50% loss of cell density in the central retina and a 33% loss in the peripheral retina compared to the control group (Fig. 4C). There was no change in the loss of DAC density at either central or peripheral areas between P17 and P25 OIR retinas (Central, $P = 0.182$; peripheral, $P = 0.629$; 1-way ANOVA). A 47% decrease in the total number of cells at P25 (control, 577 ± 34 cells versus OIR, 303 ± 36 cells, $n = 10$ control and 12 OIR; $P < 0.001$; Fig. 4D) also was similar to the decrease observed at P17 (Fig. 3D).

To confirm that DACs do not recover following OIR, the density of DACs was examined at P42. A 64% decrease in cell density was observed in the central retina (control, 33.6 ± 2.7 cells/mm^2 versus OIR, 12.0 ± 1.7 cells/mm^2; $n = 10$ control and 14 OIR; $P < 0.001$; Fig. 4E), while a 41% decrease was observed in the peripheral retina (control, 37.0 ± 2.6 cells/mm^2 versus OIR, 21.8 ± 2.0 cells/mm^2; $n = 10$ control and 14 OIR; $P < 0.001$; Fig. 4E). At this time point, the total number of cells in OIR retinas was decreased by 54% compared to the control (control, 584 ± 20 cells versus OIR, 268 ± 39 cells, $n = 10$ control and 15 OIR; $P < 0.001$; Fig. 4F).

To determine whether loss of DACs results in a decrease in TH expression, we quantified the total amount of TH in retinas collected from OIR and control mice at P42 using Western blot. As shown in Figure 5, quantification of the Western blot revealed that levels of TH expression in OIR retinas (0.0322 ± 0.0054 units TH/unit actin, $n = 5$ samples, four retinas each, Figs. 5B, 5C) were decreased by 73% compared to the controls (0.1195 ± 0.0154 units TH/unit actin, $n = 5$ samples, four retinas each, $P < 0.001$; Figs. 5A, 5C). The percentage reduction in TH expression is approximately 19% greater than the percentage reduction in cell number (Fig. 4F), suggesting that surviving DACs either have fewer processes (leading to a decrease in the total amount of TH produced) or have reduced expression of TH activity, but normal morphology.

To determine whether surviving DACs have normal dendritic morphology, RFP-labeled DACs in control and oxygen-treated retinas were injected with neurobiotin. The morphologies observed for control and OIR cells were similar (Figs. 6A, 6B). The average total dendritic length and dendritic field area were compared, and no significant differences were found between the OIR and control groups for either dendritic field (OIR, 0.179 ± 0.080 mm^2 versus control, 0.132 ± 0.076 mm^2, $P = 0.399$, $n = 4$ control and 5 OIR cells; Fig. 6C) or total

Investigative Ophthalmology & Visual Science

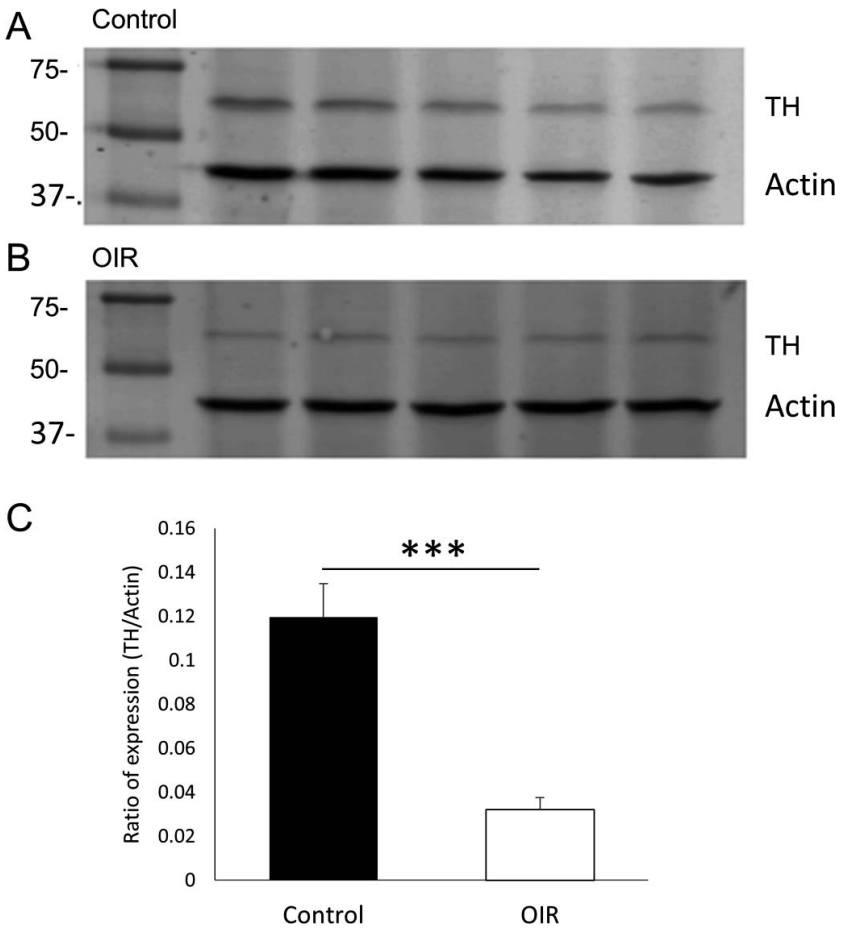

Figure 5. Retinas with OIR exhibit a significant decrease in TH expression. The level of expression of TH was estimated by Western blot using control (**A**) and OIR retinas (**B**) taken from mice at P42. The level of TH expression was decreased by 73% in OIR retinas compared to control retinas (**C**). Each *lane* contains an equal amount of protein from the homogenization of 4 retinas. The level of TH expression was normalized to the level of actin expression on a per-lane basis. Blots were scanned using the same exposure and sensitivity settings and the same exposure corrections were applied to both.

dendritic length (OIR, 1.958 ± 0.481 mm versus control, 1.742 ± 0.774 mm, $P = 0.648$, $n = 4$ control and 5 OIR cells; Fig. 6D). These results indicated that while DACs that survive OIR have normal morphology, it is likely that they express a lower amount of TH than normal.

The loss of DA cells and lowered expression of TH in surviving neurons suggests that levels of retinal dopamine are likely lowered in OIR. To test this, we measured the dopamine and DOPAC content of individual eyeballs isolated from control mice and mice with OIR at P42. Two groups of mice were used for this experiment, one of which was light-adapted and the other dark-adapted. For the dark-adapted group, mice were maintained in the dark from room lights off (7:30 PM) until noon the next day (12:00 PM) and then euthanized. For the light-adapted group, mice were euthanized on the day of the experiment 4.5 hours after lights on (12:00 AM, illuminance 300–350 lux). The results from the light-adapted group (Figs. 7A–C) show that levels of dopamine were significantly lower in oxygen-treated eyes compared to control eyes (OIR, 505.3 ± 66.6 pg/eye versus control, 1064.9 ± 88.5 pg/eye; $n = 10$ eyes; $P < 0.001$; Fig. 7A). Similarly, a substantial loss of DOPAC was observed in OIR eyes compared to control eyes (OIR, 223.5 ± 40.4 pg/eye versus control, 495.1 ± 70.9 pg/eye; $n = 10$ eyes; $P < 0.001$; Fig. 7B). The percentage of dopamine and DOPAC lost (53% and 55%, respectively) is very comparable to the percentage of DACs lost in OIR (54%), suggesting that loss of DACs is largely responsible for the decreased dopamine levels observed in OIR. In addition, we found that the ratio of DOPAC to dopamine (an indicator of dopamine release) remained unchanged in OIR (control, 0.463 ± 0.037 versus OIR, 0.456 ± 0.085, $n = 10$ control and 10 OIR eyes; $P = 0.427$; Fig. 7C), suggesting that surviving DACs can respond to light normally. Indeed, the ratio of DOPAC to dopamine in the dark-adapted OIR group (0.105 ± 0.021; $n = 6$ OIR eyes) was significantly decreased compared to that in the light-adapted group (0.389 ± 0.03; $n = 6$ eyes; $P < 0.001$; Fig. 7D).

To determine if DACs that survive OIR are physiologically normal, we used cell-attached recording to measure spontaneous and light-induced action potentials of DACs in OIR at P42 to P50. We found that DACs exhibited spontaneous action potentials in the dark (Fig. 8A). On average, the rate of action potentials was approximately 5.7 ± 1.6 Hz ($n = 7$), which is similar to that reported previously in wild-type retinas (6.1 ± 1.2 Hz).[11] When a light flash was given, an elevated number of action potentials was observed (as shown in Fig. 8B) suggesting that DACs in OIR are able to respond to light stimulation ($n = 6$). The results suggest that

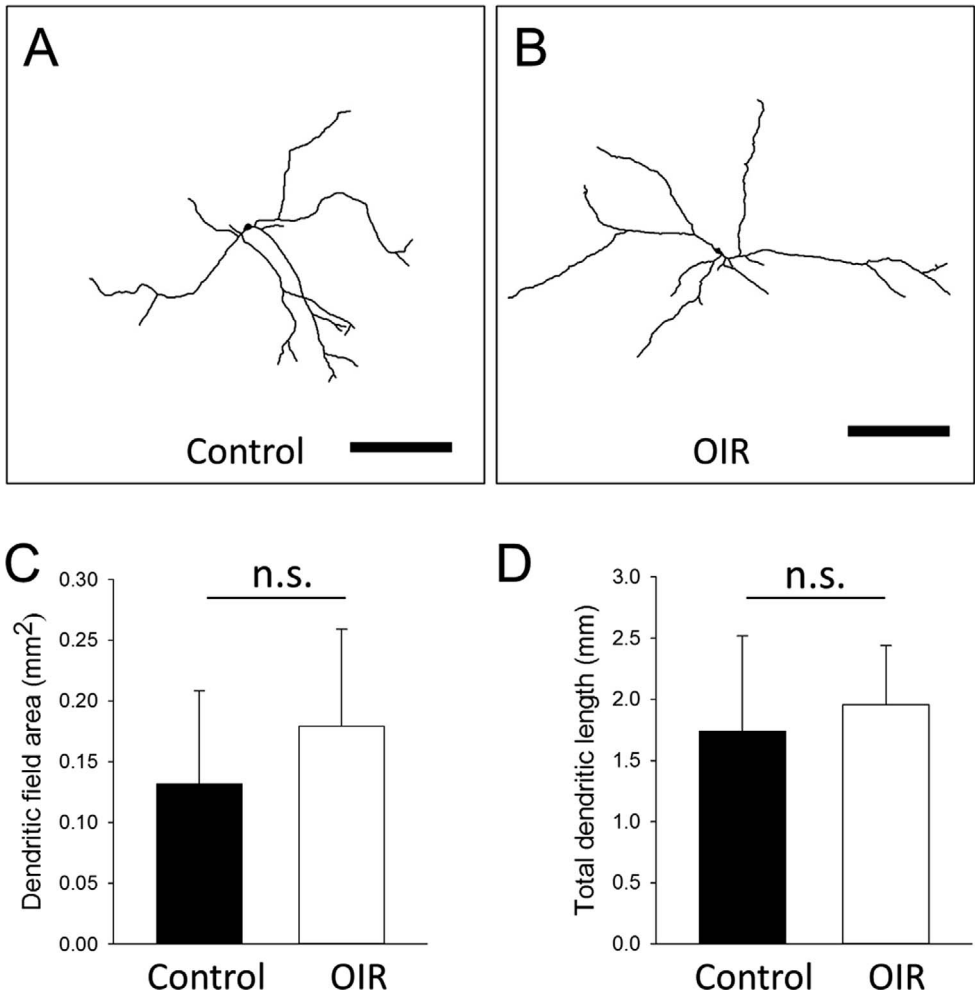

Figure 6. Dopaminergic amacrine cells that survive OIR exhibit normal morphology. Dye-injected DACs from control (**A**) and OIR (**B**) retinas exhibit similar morphologic characteristics. No significant differences were found between control and OIR cells, either in dendritic field area (**C**) or in total dendritic length (**D**). *Scale bars*: 200 μm.

in OIR, after recovery from neovascularization, DACs maintain their normal intrinsic and extrinsic properties.

Finally, we sought to determine if amacrine cells other than DACs die in OIR by immunostaining cholinergic amacrine cells. These interneurons have a key role in retinal development and in the computation of direction selectivity in the visual system. Choline acetyltransferase (ChAT) immunoreactive amacrine cells are distributed in the INL and ganglion cell layer (GCL).[17] In the INL, no significant changes in cell density were found in either central or peripheral regions between control (Figs. 9A, 9C; $n = 3$) and oxygen-treated (Figs. 9B, 9C; $n = 4$) retinas at P42 (central, control versus OIR, $P = 0.96$; peripheral: control versus OIR, $P = 0.17$). In the GCL, similarly, the cell density in the central and peripheral regions in OIR retinas remained unchanged compared to control retinas (Fig. 9C). The results suggested that, unlike DACs, cholinergic amacrine cells appear to be resistant to chronic ischemia in OIR mice.

Discussion

We demonstrated that a substantial loss of DACs occurs in mice with OIR, resulting in decreased TH immunoreactivity and decreased levels of retinal dopamine. We demonstrated further that surviving DACs have normal morphologic and physiologic properties after neovascularization has regressed spontaneously. These results suggest that surviving DACs remain with relatively normal function in OIR and that the lost DACs are primarily responsible for the decreased levels of retinal dopamine observed after OIR.

The mouse OIR model has vaso-obliteration (P7–P12) and neovascularization phases (P12–P17), which resemble the vascular changes of ROP during the progress of the disease.[12,18,19] During the vaso-obliteration phase of OIR, significant capillary dropout was observed in the central retina, which may have resulted in ischemia.[18,19] However, we were surprised to find that this did not immediately cause a reduction in the total number of TH-expressing DACs. We speculated that the heightened levels of atmospheric oxygen may have increased the amount of oxygen available to the tissues of the inner retina, keeping DACs alive.[20] Interestingly, we found that the number of TH-expressing DACs decreased substantially 5 days after mice were removed from the elevated oxygen environment, suggesting that these cells either died, lost TH immunoreactivity, or experienced morphologic alterations during the neovascularization phase. The loss of TH-expressing DACs did not reverse after the

Investigative Ophthalmology & Visual Science

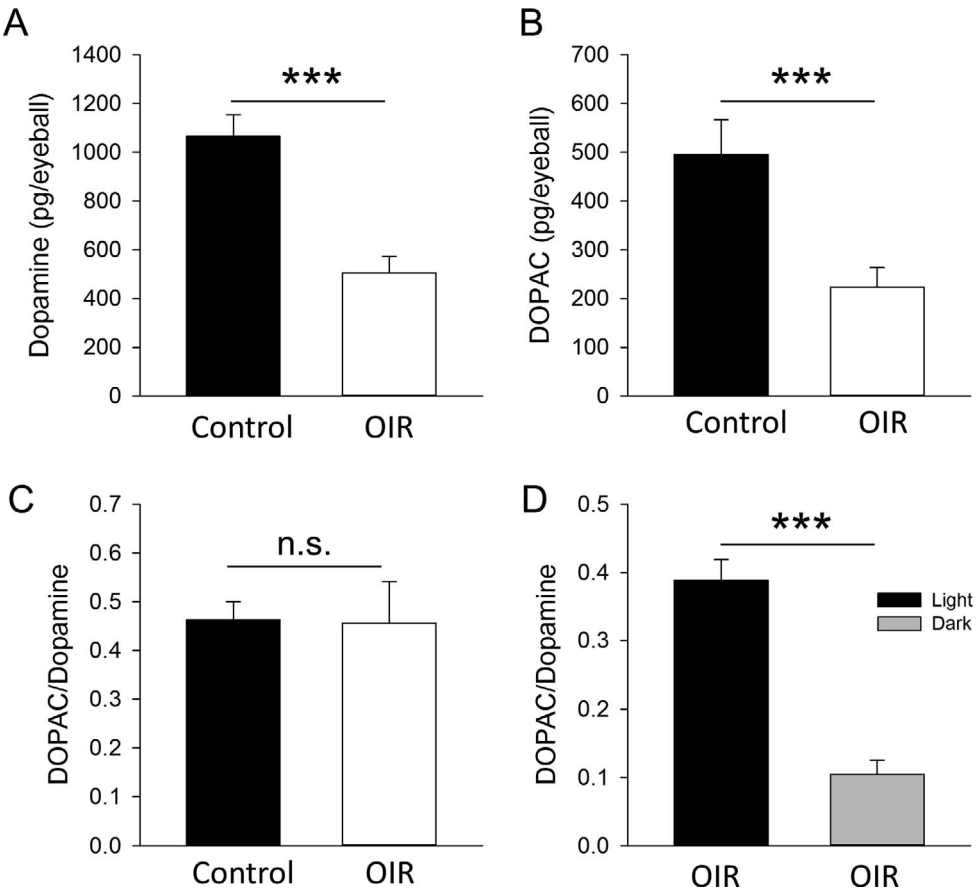

Figure 7. Effect of OIR on total dopamine and DOPAC levels. At P42, the total dopamine content of OIR eyes was determined to be 53% less than that found in control eyes (**A**). Similar results were noted for DOPAC, the primary metabolite of dopamine (**B**), while the ratio of DOPAC to dopamine (**C**) was found to remain relatively constant. The DOPAC/dopamine ratio was significantly decreased in OIR in dark-adapted eyes (**D**).

regression of neovascularization (P25 and P42), suggesting that the loss of TH-expressing DACs at P17 is likely due to the death of TH-expressing DACs, rather than downregulation of TH by ischemia. These results indicated that interventions that aim to protect DACs from death must be implemented at or before the onset of neovascularization. Missing this window would result in permanent DAC loss.

Several lines of evidence suggest that DACs that survive OIR have morphologic and functional integrity. First, surviving DACs have an unchanged dendritic field, providing a structural basis for them to form a normal network with other retinal neurons. Second, surviving DACs have relatively normal spontaneous activity and light-induced responses, suggesting that they maintain the physiologic functions that are essential for triggering dopamine release. Finally, in OIR, the ratio of DOPAC to dopamine is higher in light than in darkness, indicating that surviving DACs are able to release dopamine in response to light. The morphologic and functional integrity of surviving DACs could be involved in the preservation of visual function and eye development in OIR.

Based on these findings, we concluded that the dendrite loss previously observed in the rat OIR model[3] is due to DAC loss rather than to dendrite loss of surviving DACs. The reduction in levels of retinal dopamine observed in the present and previous work appears to be a result of DAC death.[3] While we have not attempted to test the causes of the death of DACs, previous studies have shown that dopaminergic neurons, in general, appear to be particularly vulnerable to hypoxic-ischemic insults such as oxidative and nitrosative stress and excitotoxicity resulting from increased glutamate release.[21–24] These probable causes for the death of DACs in OIR merit further investigation.

In the retina, up to 30 distinct subpopulations of amacrine cells (including DACs) have been identified based on neurotransmitter type, dendritic morphology, and/or functional characteristics.[25,26] In addition to DACs, a previous study has reported the death of AII amacrine cells (critical interneurons that transmit rod signals from the rod pathway to the cone pathway) in a rat model of OIR.[10] However, we did not find a change in the number of cholinergic amacrine cells. In addition, other amacrine, horizontal, bipolar, and retinal ganglion cells are not, or are much less, vulnerable to OIR than DACs and AII amacrines.[10,27–31] Therefore, it appears that DACs and AII amacrine cells are among the cell types most vulnerable to OIR.

The death of DACs and decreased levels of retinal dopamine reported have important implications for understanding the visual deficits associated with ROP. Visual deficits are evidenced by abnormalities of the ERG, in particular the deterioration of ERG Ops.[8,9,31,32] Since DACs may be involved in the generation of Ops,[7–9] fewer DACs or decreased dopamine levels may lead to the decreased amplitude of Ops previously reported in OIR animal models and patients with ROP.

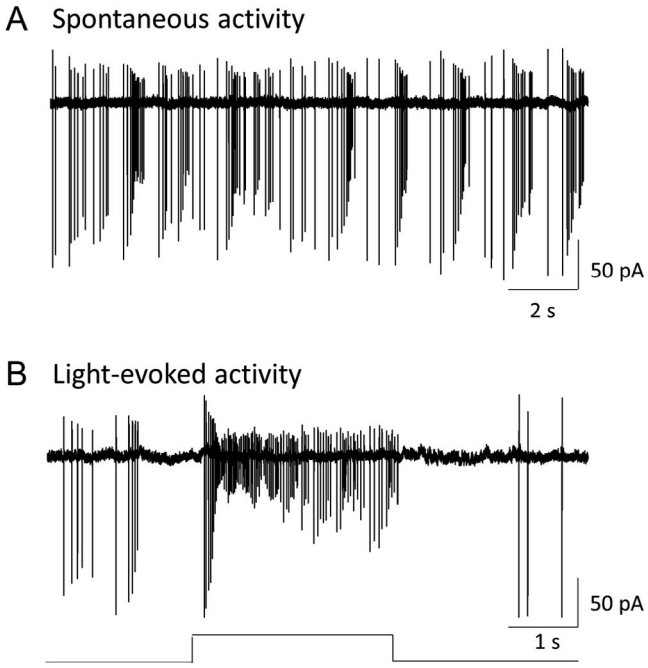

Figure 8. Dopaminergic amacrine cells that survive OIR exhibit relatively normal electrophysiologic characteristics. Cell-attached recordings were made in voltage-clamp mode with the pipette holding a potential of 0 mV. A DAC exhibited spontaneous action potentials in the dark (**A**). (**B**) The same DAC showed an elevated number of action potentials in response to a 3-second flash (*square wave* below response trace; 470 nm; 4.7×10^{13} photons/s/cm^2).

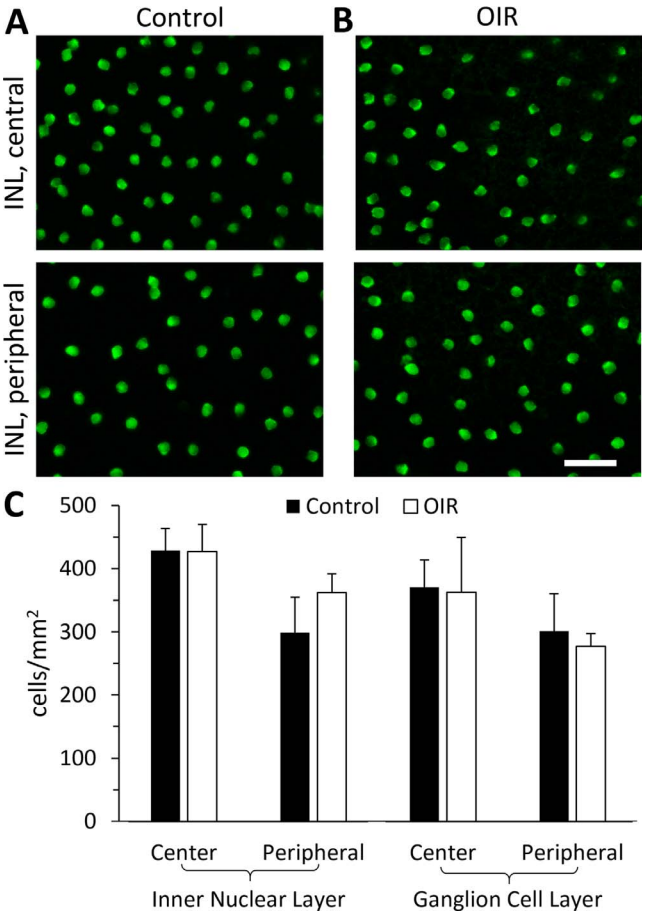

Figure 9. The number of cholinergic amacrine cells remains unchanged in OIR. (**A**) Images taken from the central (*top*) and peripheral (*bottom*) regions of the INL in a control retina. (**B**) Images taken from the central (*top*) and peripheral (*bottom*) areas of the INL in an OIR retina. *Scale bar*: 40 μm. The number of cholinergic amacrine cells in the central and peripheral regions of the INL appears to be unaffected by OIR as indicated by averaged data in (**C**). Averaged data in (**C**) also show that OIR did not change the cell density in either central or peripheral regions of the GCL.

Low levels of dopamine also have been considered as a cause of myopia in OIR or ROP.[3,4,33,34] In contrast to other myopia models, OIR myopia has a short axial length with increased corneal power and lens power.[4] Apparently, the increased anterior segment power is the cause of OIR myopia. The influence of dopamine on anterior segment development remains unknown, but a study using mouse developmental glaucoma models indicates that dopamine precursor L-3,4-dihydroxyphenylalanine is likely involved in anterior segment dysgenesis.[35] Future research is needed to explore the role of dopamine in anterior segment development, especially as it pertains to myopia in OIR.

Acknowledgments

The authors thank Kenneth Mitton, PhD, and Mei Cheng for their generous assistance.

Supported by Oakland University Provost's Undergraduate Student Research Awards (NJS and JPH), and NIH Grants EY022640 (D-QZ), EY018640 (CPR), and EY010608 (Vision core grant for the Ruiz Department of Ophthalmology), the Hermann Eye Fund (CPR and Ruiz Department of Ophthalmology), and Research to Prevent Blindness through a Challenge Grant (Ruiz Department of Ophthalmology).

Disclosure: **N.J. Spix,** None; **L.-L. Liu**, None; **Z. Zhang**, None; **J.P. Hohlbein**, None; **C.L. Prigge,** None; **S. Chintala**, None; **C.P. Ribelayga**, None; **D.-Q. Zhang**, None

References

1. Witkovsky P. Dopamine and retinal function. *Doc Ophthalmol*. 2004;108:17–40.
2. McMahon DG, Iuvone PM, Tosini G. Circadian organization of the mammalian retina: from gene regulation to physiology and diseases. *Prog Retin Eye Res*. 2014;39:58–76.
3. Zhang N, Favazza TL, Baglieri AM, et al. The rat with oxygen-induced retinopathy is myopic with low retinal dopamine. *Invest Ophthalmol Vis Sci*. 2013;54:8275–8284.
4. Chui TY, Bissig D, Berkowitz BA, Akula JD. Refractive development in the "ROP rat." *J Ophthalmol*. 2012;2012:956705.
5. Wang J, Ren X, Shen L, Yanni SE, Leffler JN, Birch EE. Development of refractive error in individual children with regressed retinopathy of prematurity. *Invest Ophthalmol Vis Sci*. 2013;54:6018–6024.
6. Wulle I, Schnitzer J. Distribution and morphology of tyrosine hydroxylase-immunoreactive neurons in the developing mouse retina. *Brain Res*. 1989;48:59–72.
7. Heynen H, Wachtmeister L, van Norren D. Origin of the oscillatory potentials in the primate retina. *Vision Res*. 1985;25:1365–1373.
8. Liu K, Akula JD, Hansen RM, Moskowitz A, Kleinman MS, Fulton AB. Development of the electroretinographic oscillato-

ry potentials in normal and ROP rats. *Invest Ophthalmol Vis Sci*. 2006;47:5447–5452.

9. Akula JD, Mocko JA, Moskowitz A, Hansen RM, Fulton AB. The oscillatory potentials of the dark-adapted electroretinogram in retinopathy of prematurity. *Invest Ophthalmol Vis Sci*. 2007; 48:5788–5797.
10. Downie LE, Hatzopoulos KM, Pianta MJ, et al. Angiotensin type-1 receptor inhibition is neuroprotective to amacrine cells in a rat model of retinopathy of prematurity. *J Compar Neurol*. 2010;518:41–63.
11. Zhang DQ, Zhou TR, McMahon DG. Functional heterogeneity of retinal dopaminergic neurons underlying their multiple roles in vision. *J Neurosci*. 2007;27:692–699.
12. Smith LE, Wesolowski E, McLellan A, et al. Oxygen-induced retinopathy in the mouse. *Invest Ophthalmol Vis Sci*. 1994;35: 101–111.
13. Zhang DQ, Stone JF, Zhou T, Ohta H, McMahon DG. Characterization of genetically labeled catecholamine neurons in the mouse retina. *Neuroreport*. 2004;15:1761–1765.
14. Preibisch S, Saalfeld S, Tomancak P. Globally optimal stitching of tiled 3D microscopic image acquisitions. *Bioinformatics*. 2009;25:1463–1465.
15. Longair MH, Baker DA, Armstrong JD. Simple Neurite Tracer: open source software for reconstruction, visualization and analysis of neuronal processes. *Bioinformatics*. 2011;27: 2453–2454.
16. Zhang J, Yang Z, Wu SM. Development of cholinergic amacrine cells is visual activity-dependent in the postnatal mouse retina. *J Compar Neurol*. 2005;484:331–343.
17. Jeon CJ, Strettoi E, Masland RH. The major cell populations of the mouse retina. *J Neurosci*. 1998;18:8936–8946.
18. Connor KM, Krah NM, Dennison RJ, et al. Quantification of oxygen-induced retinopathy in the mouse: a model of vessel loss, vessel regrowth and pathological angiogenesis. *Nat Protoc*. 2009;4:1565–1573.
19. Scott A, Fruttiger M. Oxygen-induced retinopathy: a model for vascular pathology in the retina. *Eye (Lond)*. 2010;24:416–421.
20. Pournaras CJ, Tsacopoulos M, Riva CE, Roth A. Diffusion of O2 in normal and ischemic retinas of anesthetized miniature pigs in normoxia and hyperoxia. *Graef's Arch Clin Exp Ophthalmol*. 1990;228:138–142.
21. Roufail E, Harding R, Tester M, Rees S. Chronic hypoxemia: effects on developing nitrergic and dopaminergic amacrine cells. *Invest Ophthalmol Vis Sci*. 1999;40:1467–1476.
22. Loeliger M, Duncan J, Louey S, Cock M, Harding R, Rees S. Fetal growth restriction induced by chronic placental insufficiency has long-term effects on the retina but not the optic nerve. *Invest Ophthalmol Vis Sci*. 2005;46:3300–3308.
23. Seki M, Tanaka T, Nawa H, et al. Involvement of brain-derived neurotrophic factor in early retinal neuropathy of streptozotocin-induced diabetes in rats: therapeutic potential of brain-derived neurotrophic factor for dopaminergic amacrine cells. *Diabetes*. 2004;53:2412–2419.
24. Dijk F, Kamphuis W. An immunocytochemical study on specific amacrine cell subpopulations in the rat retina after ischemia. *Brain Res*. 2004;1026:205–217.
25. Masland RH. The tasks of amacrine cells. *Vis Neurosci*. 2012; 29:3–9.
26. Masland RH. Neuronal diversity in the retina. *Curr Opin Neurobiol*. 2001;11:431–436.
27. Tokunaga CC, Chen YH, Dailey W, Cheng M, Drenser KA. Retinal vascular rescue of oxygen-induced retinopathy in mice by norrin. *Invest Ophthalmol Vis Sci*. 2013;54:222–229.
28. Dorfman AL, Cuenca N, Pinilla I, Chemtob S, Lachapelle P. Immunohistochemical evidence of synaptic retraction, cytoarchitectural remodeling, and cell death in the inner retina of the rat model of oygen-induced retinopathy (OIR). *Invest Ophthalmol Vis Sci*. 2011;52:1693–1708.
29. Mehdi MK, Sage-Ciocca D, Challet E, Malan A, Hicks D. Oxygen-induced retinopathy induces short-term glial stress and long-term impairment of photoentrainment in mice. *Graefes Arch Clin Exp Ophthalmol*. 2014;252:595–608.
30. Fletcher EL, Downie LE, Hatzopoulos K, et al. The significance of neuronal and glial cell changes in the rat retina during oxygen-induced retinopathy. *Doc Ophthalmol*. 2010;120:67–86.
31. Nakamura S, Imai S, Ogishima H, Tsuruma K, Shimazawa M, Hara H. Morphological and functional changes in the retina after chronic oxygen-induced retinopathy. *PLoS One*. 2012;7: e32167.
32. Fulton AB, Hansen RM, Moskowitz A. The cone electroretinogram in retinopathy of prematurity. *Invest Ophthalmol Vis Sci*. 2008;49:814–819.
33. Baker PS, Tasman W. Myopia in adults with retinopathy of prematurity. *Am J Ophthalmol*. 2008;145:1090–1094.
34. Cook A, White S, Batterbury M, Clark D. Ocular growth and refractive error development in premature infants without retinopathy of prematurity. *Invest Ophthalmol Vis Sci*. 2003; 44:953–960.
35. Libby RT, Smith RS, Savinova OV, et al. Modification of ocular defects in mouse developmental glaucoma models by tyrosinase. *Science*. 2003;299:1578–1581.

Investigative Ophthalmology & Visual Science